ATP-dependent motor activity of the transcription termination factor Rho from *Mycobacterium tuberculosis*

François D'Heygère[1,2], Annie Schwartz[1], Franck Coste[1], Bertrand Castaing[1,3] and Marc Boudvillain[1,3,*]

[1]Centre de Biophysique Moléculaire, CNRS UPR4301, rue Charles Sadron, 45071 Orléans cedex 2, France, [2]Ecole doctorale Santé, Sciences Biologiques et Chimie du Vivant (ED 549), Université d'Orléans, Orléans, France and [3]ITP Sciences Biologiques & Chimie du Vivant, Université d'Orléans, Orléans, France

ABSTRACT

The bacterial transcription termination factor Rho——a ring-shaped molecular motor displaying directional, ATP-dependent RNA helicase/translocase activity——is an interesting therapeutic target. Recently, Rho from *Mycobacterium tuberculosis* (ₘₜᵦRho) has been proposed to operate by a mechanism uncoupled from molecular motor action, suggesting that the manner used by Rho to dissociate transcriptional complexes is not conserved throughout the bacterial kingdom. Here, however, we demonstrate that ₘₜᵦRho is a *bona fide* molecular motor and directional helicase which requires a catalytic site competent for ATP hydrolysis to disrupt RNA duplexes or transcription elongation complexes. Moreover, we show that idiosyncratic features of the ₘₜᵦRho enzyme are conferred by a large, hydrophilic insertion in its N-terminal 'RNA binding' domain and by a non-canonical R-loop residue in its C-terminal 'motor' domain. We also show that the 'motor' domain of ₘₜᵦRho has a low apparent affinity for the Rho inhibitor bicyclomycin, thereby contributing to explain why *M. tuberculosis* is resistant to this drug. Overall, our findings support that, in spite of adjustments of the Rho motor to specific traits of its hosting bacterium, the basic principles of Rho action are conserved across species and could thus constitute pertinent screening criteria in high-throughput searches of new Rho inhibitors.

INTRODUCTION

RNA helicases are ubiquitous motor proteins that remodel RNA and RNA-protein structures and are involved in all steps of RNA metabolism (1,2). Their activities are often implicated in infection and disease and thus constitute attractive prognostic/diagnostic markers or potential drug targets (3). RNA helicases generally rely on one of two distinct mechanisms of action (1,4). Some RNA helicases are directional, NTP-fueled translocase enzymes exhibiting some degree of processivity. In this case, the helicase loads onto a single-stranded RNA segment and then uses the energy derived from ATP hydrolysis to migrate toward one end of the RNA chain, removing bound obstacles (such as a complementary strand) from its path. This mechanism is reminiscent of that used by DNA helicases (5). Other RNA helicases are local 'disruptases' that load on RNA and remodel/disrupt its local structure (or local interaction with an RNA-binding protein) in an ATP-dependent fashion. In this case, the RNA helicase acts as a non-directional and non-processive molecular switch. Local 'disruptases' are best exemplified by DEAD-box proteins which compose the largest group of RNA helicases. Upon ATP binding, DEAD-box proteins adopt a tight RNA-bound, 'close' state able to denature local RNA structures; upon release of the products of ATP hydrolysis, they revert to an RNA-free 'open' state allowing enzyme recycling (1,6).

The bacterial transcription termination factor Rho is an important model of ring-shaped helicase (4,5). Rho unwinds deleterious RNA:DNA duplexes (R-loops) that are formed behind RNA polymerase (RNAP) during transcription and dissociates transcription elongation complexes (TECs) at specific loci of bacterial genomes (7,8). The molecular mechanisms used by Rho to unwind duplexes and dissociate TECs have been studied extensively, although work has focused primarily on the Rho factor from *Escherichia coli* (ₑᵧRho) (7,9). These studies revealed that Rho uses a sophisticated translocation mechanism, called 'tethered tracking', to slide in a 5–3′ direction along nascent RNA, dissociating transcriptional R-loops and/or TECs in the process (Figure 1A). This mechanism invokes net translocation steps of one RNA base per hydrolyzed

---

*To whom correspondence should be addressed. Tel: +33 2 38 25 55 85; Fax: +33 2 38 63 15 17; Email: marc.boudvillain@cnrs-orleans.fr
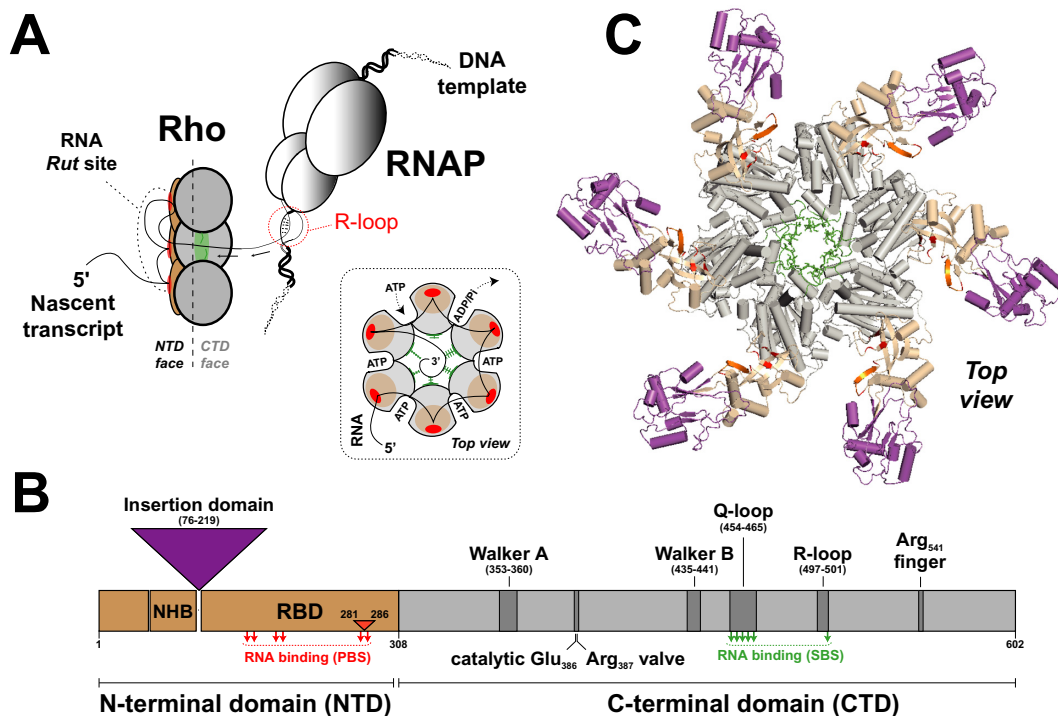
Figure 1. Transcription termination factor Rho. (**A**) A model of Rho-dependent transcription termination based on studies of $_{Ec}$Rho (7). Once bound to a C-rich *Rut* site, the Rho hexamer translocates along the nascent transcript in an ATP-dependent fashion until it catches up with RNAP and triggers dissociation of the TEC. Obstacles such as transcriptional R-loops are removed in the process. Direct contacts between Rho and RNAP, which may exist prior to Rho binding to the nascent transcript (55), are not represented here. Similarly, the exact pathway leading to TEC dissociation once Rho has caught up with the RNAP is still debated (7,8) and is not detailed here. A schematic of the RNA-bound Rho hexamer during 'tethered tracking' is also shown in the inset. (**B**) Diagram showing the arrangement of key motifs within the primary sequence of Rho subunits. The N-terminal helix bundle (NHB) domain may contribute to RNA recruitment to the Rho hexamer (36) which is ensured primarily by residues within the RNA binding domain (RBD). The large insertion domain present in $_{Mtb}$Rho (13) is depicted by a purple triangle. Amino acid numbering corresponds to the $_{Mtb}$Rho protein. PBS and SBS residues contacting RNA in $_{Ec}$Rho structures (10,37) are depicted by red and green arrows, respectively. The 6 aa insert between PBS residues of $_{Mtb}$Rho is depicted by a small orange triangle. (**C**) A model of the $_{Mtb}$Rho hexamer. An homology model of the $_{Mtb}$Rho subunit was built with Swiss-Model (http://www.swissmodel.expasy.org/) without pre-defined template. Then, the $_{Mtb}$Rho hexamer was reconstructed by aligning modeled $_{Mtb}$Rho subunits with subunits of the $_{Ec}$Rho hexamer (PDB: 3ICE) using Pymol software (http://www.pymol.org). Apart from the insertion domain, the $_{Mtb}$Rho and $_{Ec}$Rho subunits are structurally similar (rmsd ~ 1.3 Å). Color coding is the same as in panel B.

ATP molecule (10–12) and conforms to the general idea that toroidal helicases directionally translocate nucleic acids within their central channel (5).

Rho is an interesting antibacterial target because it is widespread in bacteria and absent from eukaryotes (13). Bicyclomycin (BCM), a natural Rho inhibitor used in veterinary medicine (14), is mostly effective against Gram-negative bacteria (15). Until now, only one Gram-positive species—*Micrococcus luteus*—has been found to be sensitive to BCM (16). Bacterial resistance to BCM may have several origins. Rho may be dispensable in (as for *Staphylococcus aureus*) (17) or absent from (as for ∼8% of bacterial species) (13) a given bacterium. Alternatively, the bacterium may use a specific resistance mechanism, for instance one conferred by a drug efflux protein (18) or by mutations in Rho that alter BCM binding (13,19). It is also conceivable that the mechanism of action of Rho is different and insensitive to BCM in some bacteria. BCM binds in a subsite of the ATPase pocket of $_{Ec}$Rho where it occludes binding of the nucleophilic water molecule required for ATP hydrolysis (15,20). Thus, Rho factors that would not use ATPase-driven, molecular motor activity to trigger transcription termination would be inherently resistant to BCM.

Rho is considered essential for the growth of *Mycobacterium tuberculosis* (21–23), a species that is nonetheless resistant to BCM (24). A recent report suggests that *M. tuberculosis'* Rho ($_{Mtb}$Rho) has no duplex unwinding (helicase) activity and can dissociate TECs without efficient molecular motor action (25). The authors argue that only ATP binding to $_{Mtb}$Rho is required for its transcription termination function because non-hydrolysable adenosine 5′-(β,γ-imido)triphosphate (AMP-PNP) and ATPγS analogs stimulate the dissociation of artificially stalled TECs by $_{Mtb}$Rho. They also observed that BCM inhibits the ATPase activity of $_{Mtb}$Rho (IC$_{50}$ = 30 μM) but fails to significantly affect transcription termination in the tested concentration range (up to 200 μM of BCM) (25). These unexpected findings suggest that $_{Mtb}$Rho uses a mechanism that is different from that of $_{Ec}$Rho and reminiscent of that used by RNA helicases working as local 'disruptases'.

To test the possibility that $_{Mtb}$Rho uses a molecular switch (e.g. local 'disruptase') mechanism that would make it intrinsically resistant to BCM, we have studied the motor activity of $_{Mtb}$Rho in detail using *in vitro* ATPase, duplex unwinding and transcription termination assays as well as a catalytic $_{Mtb}$Rho mutant and $_{Mtb}$Rho/$_{Ec}$Rho do-

main fusion chimera. We show that $_{Mtb}$Rho is a [5′→3′]-directional, ATP-dependent RNA helicase which requires a catalytic site that is fully competent for ATP hydrolysis to promote duplex unwinding or transcription termination. Non-hydrolysable ATP analogs do not promote duplex unwinding by $_{Mtb}$Rho nor change dramatically $_{Mtb}$Rho affinity for RNA. Furthermore, both the helicase and transcription termination activities of $_{Mtb}$Rho can be inhibited by BCM, albeit at concentrations that are significantly higher than for $_{Ec}$Rho. Experiments with a domain deletion mutant and the $_{Mtb}$Rho/$_{Ec}$Rho chimera indicate that this low apparent BCM affinity is conferred principally by the C-terminal domain (CTD) of $_{Mtb}$Rho while the N-terminal domain (NTD) specifies which regions of nascent RNA transcripts are utilized by $_{Mtb}$Rho. Overall, our data argue against a scenario whereby $_{Mtb}$Rho would rely on a distinctive, motor-independent mechanism [25] and demonstrate that $_{Mtb}$Rho is an ATP-dependent translocase that is well adapted to the peculiar transcriptome and slow metabolism of *M. tuberculosis*. Our findings also suggest that inhibition of the ATPase-dependent activities of $_{Mtb}$Rho could be a valid strategy in search of new antibiotics targeting *M. tuberculosis*.

MATERIALS AND METHODS

Materials

Chemicals and enzymes were purchased from Sigma-Aldrich and New England Biolabs, respectively. BCM was purchased from Santa Cruz Biotechnology. Sigma-saturated RNAP from *E. coli* was obtained from Epicentre Biotechnologies. Nucleoside triphosphates were purchased from GE-Healthcare while ADP, AMP-PNP and ATPγS analogs were from Sigma-Aldrich. Radionucleotides were from PerkinElmer. Synthetic oligonucleotides were obtained from Eurogentec. Polynucleotide fragment (> 300 nt) stocks were prepared as described previously [26] from polynucleotide batches obtained from Santa Cruz Biotechnology and Midland Certified Reagent Company (Midland, TX, USA). Streptavidin-coated magnetic beads were from Ademtech (Pessac, France). DNA templates used in *in vitro* transcription reactions were prepared by standard PCR procedures, as described previously [27]. RNA substrates were obtained by *in vitro* transcription of PCR amplicons with T7 RNAP and purified by denaturing polyacrylamide gel electrophoresis (PAGE), as described [26]. Plasmids for over-expression of single-point $_{Mtb}$Rho mutants were prepared by Quickchange (Stratagene) mutagenesis of the pET28b-MtbRho plasmid (kindly provided by Dr. Ranjan Sen, Hyderabad, India). Plasmids for over-expression of the Δ_{Mtb}Rho deletion mutant (wherein amino acids 76–219 of $_{Mtb}$Rho are replaced by a Val-Pro dipeptide) and the $_{[Mtb:Ec]}$Rho (wherein amino acids 1–308 of $_{Mtb}$Rho are fused to amino acids 131–419 of $_{Ec}$Rho) and $_{[Ec:Mtb]}$Rho (wherein amino acids 1–130 of $_{Ec}$Rho are fused to amino acids 309–602 of $_{Mtb}$Rho) chimeras were obtained by inserting synthetic DNA fragments (obtained by overhang extension PCR using the pET28b-Rho [26] and/or pET28b-MtbRho plasmids as starting templates) between the NdeI and XhoI sites of the pET28b plasmid (Novagen) following

standard cloning procedures (see Supplementary Table S1 for details). The sequences of DNA templates and plasmids were verified by capillary DNA sequencing (Genoscreen, France).

Preparation of proteins

The $_{Ec}$Rho protein was prepared and purified as described previously [26]. Wild-type (WT) and mutant $_{Mtb}$Rho factors as well as Mtb:Ec protein chimeras were over-expressed as N-terminal His tag fusions [25] in Rosetta 2(DE3) cells (Merck-Millipore) harboring the appropriate pET28b derivative and were purified following published procedures [28]. Briefly, the $_{Mtb}$Rho proteins were affinity selected on His-Pur colbalt resin (Thermo scientific) and were subsequently purified by cation exchange chromatography on a SP sepharose FF column (GE-Healthcare) with a 0.15–1M NaCl gradient and by gel filtration chromatography on a Sephacryl S-300 HR column (GE-Healthcare) equilibrated in GF buffer (150 mM NaCl, 20 mM HEPES, pH 7.5, 2 mM β-mercaptoethanol). Protein preparations were controlled by liquid chromatography high-resolution mass spectrometry using an UltiMate 3000 NanoRSLC system (Dionex, Sunnyvale, CA, USA) connected to a 4-GHz MaXis ultra-high resolution quadrupole-TOF spectrometer (Bruker Daltonics) equipped with an electrospray ion source. All proteins were stored at $-20°$C as micromolar solutions in 100 mM KCl, 10 mM Tris-HCl, pH 7.9, 0.1 mM EDTA, 0.1 mM DTT and 50% (v/v) glycerol. Concentrations of $_{Ec}$Rho and $_{Mtb}$Rho proteins are expressed in hexamers throughout the manuscript. Purified Ded1 protein was kindly provided by Prof. Eckhard Jankowsky (Case Western Reserve University, Cleveland, USA).

Preparation of duplex substrates

Duplexes were assembled by mixing 10 pmoles of RNA transcript with 12 pmoles of complementary oligonucleotide (bearing a 6-carboxyfluorescein label at the 5′-end) in annealing buffer (150 mM potassium acetate, 20 mM HEPES, pH 7.5, 1 mM EDTA). Mixtures were heated at 95°C and slowly cooled to 20°C. Duplexes were then purified by native 7% PAGE and stored at $-20°$C in helicase buffer (20 mM HEPES, pH 7.5, 0.1 mM EDTA, 0.5 mM DTT and 150 mM potassium glutamate) [26].

NTP hydrolysis assay

The NTP hydrolysis activities of the Rho enzymes were determined with the EnzCheck Phosphate Assay kit (Molecular Probes) as described previously [27,28]. Briefly, two quartz cuvettes containing equal volumes of a solution of 20 nM Rho, RNA cofactor (e.g. poly[rC] at a standard concentration of 10μM in rC residues), 0.4 mM 2-amino-6-mercapto-7-methylpurine riboside and 1 U/mL of purine nucleoside phosphorylase in NTPase buffer (1 mM MgCl$_2$, 50 mM Tris-HCl, pH 7.5, 0.1mM sodium azide) were placed in the control and sample beam holders of an Uvikon-XL UV-spectrophotometer equipped with a 37°C circulating water bath. After equilibration at 37°C for 5 min, equal volumes of water and NTP (1 mM, final concentration)

were added, respectively, to the control and reaction cuvettes and absorbance at 360 nm was recorded as a function of time. The NTPase rates were deduced from the initial first-derivative maxima that were obtained after smoothing of the time-dependent A_{360} curves with Kaleidagraph software. The experiments were calibrated with standard samples containing known amounts of phosphate, as recommended by the kit manufacturer.

Equilibrium binding assays

Equilibrium Rho-RNA dissociation constants were determined using a filter-binding assay, as described previously (29,30). Briefly, ~10 fmoles of ^{32}P-labeled RNA substrate were mixed with various amounts of Rho in 100 µl of binding buffer (20 mM HEPES, pH 7.5, 0.1 mM EDTA, 0.5 mM DTT, 150 mM potassium acetate and 20 µg/ml BSA) containing 0 or 1 mM ATP (or AMP-PNP). After incubation for 10 min at 30°C, the samples were filtered through stacked [top] nitrocellulose (Amersham Protran) and [bottom] cationic nylon (Pall Biodyne B) membranes using a Bio-dot SF apparatus (Biorad). No significant differences were observed in control experiments performed with 30 min incubation times (not shown). The fractions of free and Rho-bound RNA (retained on the nylon and nitrocellulose membranes, respectively) as a function of Rho concentration were then determined by phosphorimaging of the membranes using a Typhoon-Trio imager and dedicated ImageQuant TL v8.1 software (GE healthcare).

Duplex unwinding assay

Helicase reactions were performed as described previously (31) with 6-carboxyfluorescein labeled duplex substrates (control experiments with ^{32}P-labeled substrates supported that the fluorescein moiety does not affect $_{Mtb}$Rho behavior) (28). Briefly, 5 nM substrate was mixed with 50 or 500 nM Rho and 0–300 µM BCM in helicase buffer and incubated for 3 min at 30°C. Then, 1 mM MgCl$_2$, 1 mM nucleotide cofactor (ATP, ADP, ATPγS, AMP-PNP, ADP-BeF$_x$ or ADP-AlF$_4$) and 400 nM oligo trap (unlabeled oligonucleotide having the same sequence than the released 'reporter' strand) were added to the helicase mixture before further incubation at 30°C. Reaction aliquots were taken at various times and mixed with two volumes of quench buffer (10 mM EDTA, 1.5% SDS, 300 mM sodium acetate, 6% Ficoll-400) before being loaded on 9% polyacrylamide gels that contained 1X TBE and 0.5% SDS. Detection and quantification of gel bands were performed by fluorescence imaging with a Typhoon-Trio imager as described (28). Helicase reaction parameters were obtained by fitting data points to an equation describing the kinetic regimen uncovered previously for $_{Ec}$Rho:

$$F_{p} = A \times (1 - e^{-k_{exp}t}) + k_{lin} \times t$$

where F_{p} is the fraction of product formed, A is the amplitude of the exponential (burst) phase of the reaction, and k_{exp} and k_{lin} are the rate constants of the exponential and linear phases of the reaction, respectively (30,32).

Transcription termination experiments

Transcription termination experiments were performed under single-round 'chase' conditions as described previously (33) with minor modifications. Briefly, biotinylated DNA templates were prepared by PCR amplification of pT7A1-λ*cro* DNA template (34) using a 5'-biotinylated reverse primer. To allow preparation of TECs halted at +24, a forward mutagenic PCR primer was also used to introduce a C→T mutation at position +6 of the pT7A1-λ*cro* DNA template. The resulting mAS97Bt template (30 nM) was mixed with *E. coli* RNAP holoenzyme (36 nM) in transcription initiation buffer (40 mM Tris-HCl, pH 7.9, 50 mM KCl, 5 mM MgCl$_2$, 1mM DTT, 0.05 mg/ml BSA, 0.4U/µl Superase-In [Ambion]) and incubated at 37°C for 5 min. The mixture was then supplemented with 12 µM ApU, 6 µM ATP, 6µM GTP, 0.95µM UTP, and 1 µCi/µl [α^{32}P]-UTP and incubated for 10 min at 37°C. Then, the mixture was chilled on ice, KCl concentration was raised to 0.1 M and the halted transcription complexes were purified by filtration through a microspin G50 column pre-equilibrated with transcription elongation buffer (40 mM Tris-HCl, pH 7.9, 100 mM KCl, 5 mM MgCl$_2$, 1 mM DTT, 0.1 mg/ml BSA, 0.2U/µl Superase-In). The complexes were then immobilized on streptavidin beads (Supplementary Figure S4) or used directly in single-run chase reactions. In the latter case, an aliquot of the solution of halted transcription complexes (~15 nM) was supplemented with 70 nM Rho and 0–750 µM BCM in transcription elongation buffer and incubated for 10 min at 37°C. Then, rNTPs (75 µM each, final concentrations) and rifampicin (25 µg/ml) were added to initiate chase reactions. After incubation for 10 min at 37°C, the mixtures were mixed with 1 volume of denaturing buffer (95% formamide, 50 mM EDTA) and resolved by 8–10% denaturing PAGE. Gels were analyzed by Typhoon-Trio phosphorimaging. Apparent global termination efficiencies (TE$_{app}$) were defined as:

$$TE_{app} = \frac{\sum I_{term}}{\sum I_{term} + \sum I_{runoff}} \times 100$$

where $\sum I_{term}$ is the sum of the intensities of the bands corresponding to termination products while $\sum I_{runoff}$ is the sum of the intensities of the bands corresponding to runoff products. IC$_{50}$ values for BCM inhibition were obtained by non-linear least-square fitting of TE$_{app}$ values obtained as a function of BCM concentration to a standard sigmoid inhibition equation:

$$TE_{app} = (TE_{app})_0 - F_{max} \times \frac{[BCM]^n}{[BCM]^n + [IC_{50}]^n}$$

where $(TE_{app})_0$ is the value of TE$_{app}$ at 0 µM BCM, F_{max} is the maximal fraction of TE$_{app}$ that is sensitive to BCM inhibition and n is an empirical parameter that defines the sigmoid shape of inhibition (35).

Data reporting

All data values are reported as mean ± standard deviation calculated from at least two independent experimental replicates (whenever number of replicates $N_R > 2$ is indicated in figure legends).

RESULTS

Selection of protein mutants and chimeras to probe $_{Mtb}$Rho features

The typical $_{Ec}$Rho ring is made of six identical protein subunits, each divided in two distinct domains (7–9,36,37). The NTD contains primary binding site (PBS) motifs involved in the recruitment of RNA *Rut* (Rho utilization) sites by the Rho hexamer (Figure 1A and B). PBS motifs include residues forming a cleft only large enough to accommodate a 5′-YC dimer (Y and C being pyrimidine and cytosine residues, respectively), thereby explaining the preference of $_{Ec}$Rho for single-stranded C-rich *Rut* sites (7–9,37). The CTD contains residues required for intersubunit cohesion and for 'molecular motor' function. Essential CTD motifs include Walker A and B motifs forming the ATP binding pockets at subunit interfaces, 'catalytic Glu', 'Arg valve' and 'Arg finger' residues required for the catalysis of ATP hydrolysis as well as Q-loop and R-loop residues forming the secondary binding site (SBS) for RNA (Figure 1B) (10,38). Importantly, changes in the chemical state of the ATPase pockets are allosterically transmitted up to the SBS residues which are in charge of RNA translocation within the central ring channel (Figure 1A) (10).

Alignment of Rho sequences from over 1200 bacterial species indicates that most of these key residues are conserved across the bacterial kingdom, including in phylodistinct Rho factors such as $_{Mtb}$Rho (Supplementary Figure S1) (13). Notwithstanding, $_{Mtb}$Rho displays a few distinctive features that could explain its uncharacteristic behavior. These features include (i) a 144 amino acids (aa) insertion subdomain in the NTD (Figure 1 B) that should result in bulky appendages to the hexameric ring (Figure 1C, in magenta); (ii) a short insert (aa 281–286) between PBS residues (Figure 1B and Supplementary Figure S1) that could affect the structure of the 5′-YC binding clefts (Figure 1C, in red) and recognition of *Rut* sites; and (iii) a threonine instead of a lysine at an SBS position in the R-loop (Thr$_{501}$ in $_{Mtb}$Rho versus Lys$_{326}$ in $_{Ec}$Rho; Supplementary Figure S1 and Figure 1C, in green) that could weaken the allosteric interaction network critical for Rho mechanochemistry.

To probe the effect of these distinctive features, we prepared $_{Mtb}$Rho derivatives containing a single-point SBS mutation (T501A and T501K mutants) or lacking the NTD insertion subdomain (Δ_{Mtb}Rho) and a protein chimera wherein the NTD of $_{Mtb}$Rho is fused to the CTD of $_{Ec}$Rho ($_{[Mtb:Ec]}$Rho chimera). Multiple attempts to prepare the 'reverse' $_{[Ec:Mtb]}$Rho chimera (NTD of $_{Ec}$Rho fused to the CTD of $_{Mtb}$Rho) were unsuccessful because this protein was invariably expressed in inclusion bodies and could not be purified in a soluble form under native conditions (data not shown).

To probe the role of ATP hydrolysis in $_{Mtb}$Rho, we also prepared a single-point mutant wherein the catalytic glutamate residue Glu$_{386}$ is replaced by alanine (E386A mutant). The role of the catalytic glutamate residue is to polarize the nucleophilic water molecule for attack of the γ-phosphoryl group of ATP (10). The non-conservative mutation of this critical residue in $_{Ec}$Rho (E211A mutation)
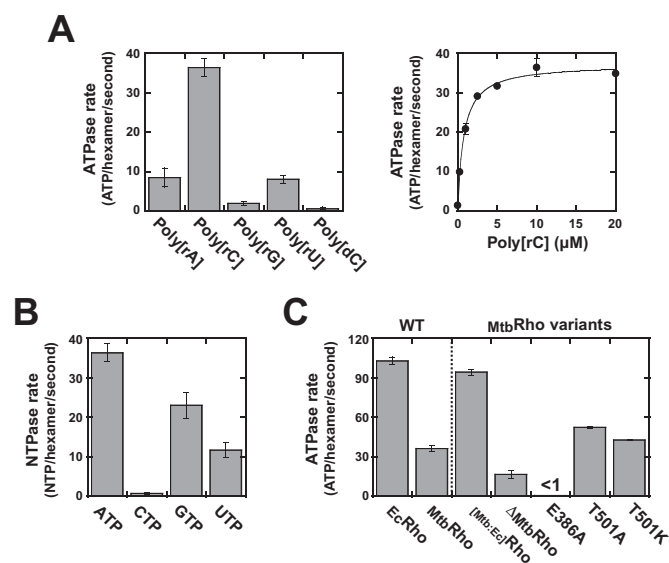

Figure 2. RNA-dependent NTP hydrolysis activities of the $_{Mtb}$Rho protein variants. Unless specified otherwise, the concentrations of NTP and RNA polymer were 1 mM and 10 μM (in nucleotide residues), respectively. (**A**) Stimulation of the ATPase activity of WT $_{Mtb}$Rho by polyribonucleotide cofactors (number of replicates, N_R = 4 for 10 μM poly[rC]). (**B**) WT $_{Mtb}$Rho hydrolyzes ATP most efficiently in the presence of poly[rC] (N_R = 4 for ATP). (**C**) Comparison of the ATPase rate of WT $_{Mtb}$Rho with rates measured under the same standard conditions for WT $_{Ec}$Rho and $_{Mtb}$Rho variants (N_R = 3 for Δ_{Mtb}Rho and N_R = 4 for WT $_{Mtb}$Rho).

does not affect ATP binding or protein oligomerization but completely abolishes ATP hydrolysis (38).

Tight allosteric coupling within the $_{Mtb}$Rho enzyme

To assess the substrate/cofactor preferences of $_{Mtb}$Rho, we performed standard measurements of its NTP hydrolysis rate (27) in the presence of various NTP substrates and polynucleotide cofactors. In agreement with previous reports (25,39), we found that an RNA cofactor is required to activate NTP hydrolysis by $_{Mtb}$Rho (Figure 2A and data not shown). Poly[rC] is the preferred polynucleotide cofactor with a K_m of ~0.7 μM (Figure 2A) while ATP is the preferred substrate (Figure 2B). Hydrolysis of CTP is highly inefficient (Figure 2B) at a concentration (1 mM) that is saturating for ATP ($K_{m, ATP} \sim 70$ μM) (25), a feature that has also been observed for the Rho factors of *M. luteus* ($_{Mlut}$Rho) (40) and *Streptomyces lividans* (41), two evolutionary relatives. By contrast, the phylodivergent $_{Ec}$Rho displays little preference for a specific NTP (40).

Under our standard conditions (see 'Materials and Methods' section), the rate of ATPase turnover is about 3-fold lower for $_{Mtb}$Rho than for $_{Ec}$Rho or for the $_{[Mtb:Ec]}$Rho chimera (Figure 2C), suggesting that components in the CTD of $_{Mtb}$Rho are suboptimal. Deletion of the NTD insertion subdomain of $_{Mtb}$Rho (Δ_{Mtb}Rho) reduces the ATPase rate by half under standard conditions (Figure 2C). However, a higher concentration of poly[rC] cofactor is required to reach maximal ATPase turnover with the Δ_{Mtb}Rho variant (data not shown), which is consistent with an RNA binding defect induced by the deletion of the NTD subdomain (see Table 1 and below). At saturating poly[rC]

concentrations, Δ_{Mtb}Rho hydrolyzes ATP at a rate of ~80 molecules per hexamer and per second, which is about twice faster than WT $_{Mtb}$Rho (Figure 2C) and suggests that the NTD subdomain somewhat contributes to regulate ATP consumption.

Altering the identity of Thr$_{501}$ in $_{Mtb}$Rho increases the rate of ATP hydrolysis by 1.2–1.4-fold (Figure 2C, T501A and T501K mutations). This modest effect suggests that Thr$_{501}$ has a less important role in $_{Mtb}$Rho than has the corresponding Lys$_{326}$ side chain in the R-loop of $_{Ec}$Rho (the K326A mutation reduces the ATPase activity of $_{Ec}$Rho by ~75%) (10,27). In sharp contrast, non-conservative mutation of the catalytic Glu$_{386}$ residue (E386A mutant) completely inhibits ATP hydrolysis by $_{Mtb}$Rho, even when concentrations of ATP and poly[rC] are increased to 5 and 30 μM, respectively (Figure 2C and data not shown). This dramatic effect induced by the E386A mutation is not matched by a drastic change of the oligomeric state or capacity to bind ATP or RNA (Supplementary Figure S2 and Table 1). Thus, the E386A phenotype is comparable to that of the inactivating E211A mutation in $_{Ec}$Rho (38) which supports that the conserved catalytic glutamate residue (Supplementary Figure S1) is also required in $_{Mtb}$Rho for polarization of the water molecule attacking the γ-phosphoryl group of ATP.

Taken together, these data establish that coupling between RNA binding and ATP hydrolysis is tight within the $_{Mtb}$Rho ring and most likely relies on similar principles in the $_{Mtb}$Rho and $_{Ec}$Rho enzymes. One should recall, however, that the rate of ATP hydrolysis is a measure of fuel consumption but by no means a measure of motor efficiency. The latter depends on multiple factors governing the mechanochemical transduction mechanism and yield (42), some of which may vary between the $_{Mtb}$Rho and $_{Ec}$Rho motors.

$_{Mtb}$Rho unwinds short RNA duplexes in a directional, ATP-dependent fashion

To probe the motor properties of $_{Mtb}$Rho, we performed duplex unwinding (helicase) experiments with model substrates (26). We prepared RNA:DNA substrates containing a 57 bp (substrate A) or 34 bp (substrate B) duplex region located downstream from a single-stranded RNA (ssRNA) tail encompassing a synthetic *Rut* site (Figure 3, inset) (30). We also prepared a 5′-ssRNA tailed substrate containing a shorter duplex (14 bp, substrate C) by pairing an oligo(2′-O-methylribonucleotide) to the RNA strand (Figure 3, inset). The 2′-O-methyl modifications, which increase RNA duplex stability significantly (43), prevent spontaneous denaturation of substrate C under our experimental conditions (Figure 3, ADP lanes in bottom gels).

We incubated each substrate with a 10-fold molar excess of Rho hexamers in the presence of ATP under 'standard' helicase reaction conditions (see 'Material and Methods' section) (30,32). As expected, $_{Ec}$Rho unwinds the three duplex substrates with high efficiencies (Figure 3, left gels and graph). Substrate C is slightly less reactive than the longer duplex substrates, probably because its 2′-O-methyl moieties favor an A-form duplex conformation and non-productive interactions with $_{Ec}$Rho (31). By contrast,
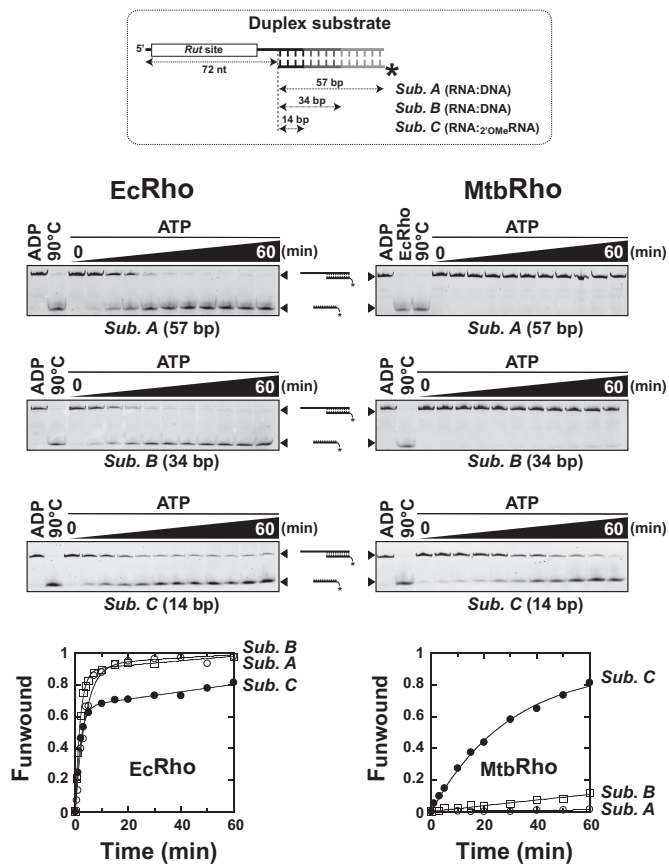

Figure 3. The $_{Mtb}$Rho helicase unwinds short duplex substrates containing a 5′-single-stranded RNA tail. The duplex substrates used in helicase assays contain a synthetic *Rut* site for $_{Ec}$Rho (30) and are schematically depicted at the top of the figure. Unwinding reactions were performed under standard conditions with 50 nM of the $_{Ec}$Rho (left) or $_{Mtb}$Rho (right) helicase and 5 nM of the indicated substrate. Representative 9% PAGE gels and fraction unwound versus time graphs illustrate the helicase activities observed in each case ($N_R = 3$ except for experiments with $_{Mtb}$Rho and substrate C [$N_R = 5$]).

$_{Mtb}$Rho unwinds substrate C most efficiently, unwinds substrate B very inefficiently, and is completely unable to unwind the 57 bp-long duplex of substrate A (Figure 3, right gels and graph). Incubation of the substrates with larger excesses (100-fold) of $_{Mtb}$Rho does not change unwinding kinetics significantly (data not shown), indicating that $_{Mtb}$Rho was already present at a saturating concentration. These data demonstrate that $_{Mtb}$Rho is a RNA helicase, albeit one that works on a narrower range of substrates than $_{Ec}$Rho.

This narrow spectrum of activity may be due to suboptimal interactions between $_{Mtb}$Rho and the substrates. Optimal *Rut* features for $_{Mtb}$Rho are currently unknown and may not be adequately represented by our synthetic *Rut* sequence (Figure 3, inset), which had been optimized for $_{Ec}$Rho (30,44). Furthermore, the interaction network promoting RNA translocation may be weakened in $_{Mtb}$Rho by the K→T substitution at position 501 of the R-loop (corresponding to SBS residue Lys$_{326}$ in $_{Ec}$Rho; see above). To test these scenarios, we performed unwinding experiments with $_{Mtb}$Rho protein variants. We observed that the $_{[Mtb:Ec]}$Rho chimera unwinds the three substrates with effi-

Table 1. RNA binding parameters[a]

Rho factor	No nucleotides		+ AMP-PNP		+ ATP	
	n	K_d (nM)	n	K_d (nM)	n	K_d (nM)
WT $_{Mtb}$Rho	1.2 ± 0.2	3.5 ± 0.7	0.9 ± 0.2	2.0 ± 0.3	1.0 ± 0.2	2.4 ± 0.6
E386A	1.5 ± 0.3	5.3 ± 0.8	0.9 ± 0.2	2.2 ± 0.4	1.1 ± 0.4	3.3 ± 1.0
Δ_{Mtb}Rho	2.3 ± 0.6	20.4 ± 2.3	1.4 ± 0.2	16.3 ± 0.4	1.7 ± 0.3	14.4 ± 1.0

[a]Values were determined from the best non-linear least square fits of binding data to the Hill equation, $F = F_\infty \times [Rho]^n/(K_d{}^n + [Rho]^n)$, where F is the fraction of labeled substrate retained on the nitrocellulose membrane, F_∞ is the maximal fraction of bound substrate, n is the Hill coefficient and K_d is the apparent dissociation constant. Experiments were performed with the *Rut*-containing RNA strand of helicase substrates (Figure 3) and the indicated $_{Mtb}$Rho variants as described in methods.
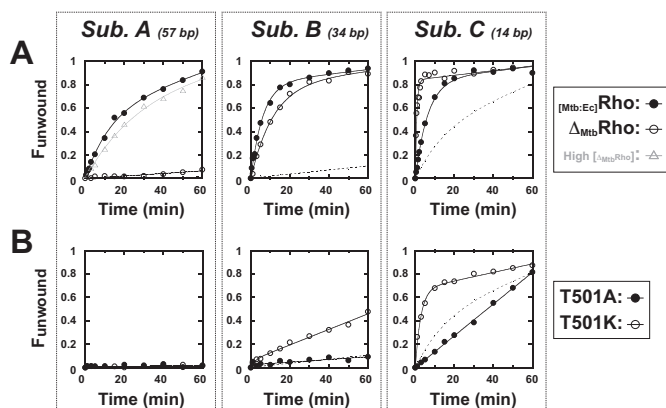

Figure 4. Helicase activities of the $_{Mtb}$Rho protein variants. Unwinding experiments were performed under standard conditions with substrate A, B or C (Figure 3, inset) and (**A**) the $_{[Mtb:Ec]}$Rho chimera and Δ $_{Mtb}$Rho deletion mutant or (**B**) single-point mutants T501A and T501K. To facilitate comparisons, reaction time-courses for WT $_{Mtb}$Rho are depicted as dotted curves.

ciencies that approach the ones displayed by $_{Ec}$Rho (Figure 4A, filled circles; compare with Figure 3). The ATPase rates of $_{[Mtb:Ec]}$Rho and $_{Ec}$Rho are also comparable (Figure 2C). These data indicate that $_{Mtb}$Rho's NTD is reasonably functional (and able to use our synthetic *Rut* sequence) when compared to $_{Ec}$Rho's NTD. Notwithstanding, deletion of the NTD insertion subdomain (Δ_{Mtb}Rho variant) also significantly increase the capacity of $_{Mtb}$Rho to unwind the 14 bp and 34 bp duplex substrates (Figure 4A, open circles). When present at a 10-fold higher concentration (500 nM), the Δ_{Mtb}Rho variant can even unwind the 57 bp duplex of substrate A with reasonable efficiency (Figure 4A, open triangles) which, as stated above, is not the case of WT $_{Mtb}$Rho. These data combined with equilibrium binding measurements (Table 1) confirm that the NTD insertion subdomain stimulates RNA binding but interferes with motor function.

The T501A and T501K mutations have distinct effects on the helicase activity of $_{Mtb}$Rho. The T501A mutant is slightly less active than the WT enzyme with the shortest (14 bp) duplex substrate and similarly inefficient with the longer duplexes (Figure 4B, filled circles). By contrast, the T501K mutant is significantly more active and able to unwind a longer (34 bp) duplex than WT $_{Mtb}$Rho (Figure 4B, open circles). Moreover, the amplitude of the exponential phase of the unwinding reaction (with Substrate C) is null for T501A but is ∼2-fold higher for T501K than for WT

(Figure 4B). It has been shown for $_{Ec}$Rho that the amplitude of the exponential phase depends on helicase processivity under similar unwinding reaction conditions (30,32). These observations suggest that stabilizing, productive contacts are formed between the R-loop and RNA within the SBS of $_{Mtb}$Rho but that these contacts are suboptimal unless Thr$_{501}$ is replaced by a lysine. Significantly, a lysine or arginine is found at the corresponding R-loop position in the Rho factors from most species (e.g. Lys$_{326}$ in $_{Ec}$Rho) (13), with the notable exception of mycobacteria and coryneform relatives (data not shown). Taken together, these findings indicate that features weakening the $_{Mtb}$Rho helicase (with respect to the $_{Ec}$Rho prototype) are located both in its N-terminal 'RNA anchoring' and in its C-terminal 'motor' domains.

Selective unwinding of short duplexes by $_{Mtb}$Rho is reminiscent of the activity of DEAD-box proteins which disrupt short RNA duplexes in a local, non-directional fashion. However, $_{Mtb}$Rho is unable to unwind a substrate C derivative wherein the relative positions of the *Rut*-containing ssRNA and 14bp duplex regions are permuted (Supplementary Figure S3). The $_{Ec}$Rho enzyme also has no [3′→5′] unwinding activity (30) whereas DEAD-box protein Ded1 unwinds substrate C and its permuted derivative with similar high efficiencies (Supplementary Figure S3), as expected (45). These data thus support that $_{Mtb}$Rho is a directional [5′→3′] helicase behaving more like the $_{Ec}$Rho translocase than the local 'disruptase' Ded1.

ATP hydrolysis is required for duplex unwinding by $_{Mtb}$Rho

A hallmark of RNA translocases is their tight dependence on NTP hydrolysis. By contrast, local disruptases such as DEAD-box proteins often do not require ATP hydrolysis to unwind short RNA duplexes provided that their RNA clamp conformation is stabilized by ATP or a non-hydrolysable ATP analog (46,47). A similar capacity has been proposed for $_{Mtb}$Rho which is able to disrupt an artificially stalled TEC in the presence of AMP-PNP or ATPγS, albeit at rates that are only, respectively, ∼7 and ∼23% of the dissociation rate measured in the presence of ATP (25). We performed RNA affinity measurements to test this proposal but observed that $_{Mtb}$Rho:RNA complexes are only marginally stabilized by nucleotides such as AMP-PNP or ATP (Table 1).

To explore the relationship between the ATPase activity and motor function of $_{Mtb}$Rho, we also carried out unwinding experiments with the 14 bp duplex substrate C (Figure 3) in the presence of various analogs of ATP. We found that non-hydrolysable ATP analogs AMP-

PNP, ADP-BeF$_x$ (ground-state mimic), and ADP-AlF$_4$ (transition-state mimic) do not promote unwinding of substrate C by $_{Mtb}$Rho (Figure 5A). Similarly, we observed that the ATPγS analog, which is hydrolyzed by $_{Mtb}$Rho at a ∼15-fold lower rate than ATP under our standard conditions (data not shown), does not stimulate the $_{Mtb}$Rho helicase significantly (Figure 5A). UTP and CTP are also highly inefficient helicase cofactors whereas GTP is only slightly less efficient than ATP at promoting unwinding of substrate C by $_{Mtb}$Rho (Figure 5A). Overall, the order of NTP efficiency is very similar for duplex unwinding (Figure 5A) and for NTP hydrolysis by $_{Mtb}$Rho (Figure 2B).

The catalytic mutant E386A does not unwind substrate C significantly (Figure 5B) which confirms that ATP hydrolysis is required for the helicase function of $_{Mtb}$Rho. Further support for this conclusion comes from the observation that BCM inhibits the $_{Mtb}$Rho helicase in a dose-dependent fashion (Figure 5C), albeit with a half-maximal inhibitory concentration (IC$_{50}$ = [157 ± 20] μM) that is higher than for $_{Ec}$Rho (IC$_{50}$ = [49 ± 5] μM). Altogether, these data support that $_{Mtb}$Rho is a *bona fide* ATP-dependent molecular motor which requires ATP hydrolysis to trigger duplex unwinding.

Transcription termination requires a catalytically-competent ATPase pocket in $_{Mtb}$Rho

To assess how the peculiar features of $_{Mtb}$Rho affect its transcription termination activity, we performed *in vitro* transcription termination experiments with the RNAP of *E. coli* and a DNA template encoding the Rho-dependent terminator λtR1 (Figure 6A) (27,34). With this heterologous model system and under single-round 'chase' conditions (see 'Material and Methods'), $_{Mtb}$Rho triggers transcription termination with a global apparent efficiency (TE$_{app}$) that is comparable to that of $_{Ec}$Rho (Figure 6B). However, the termination window (i.e. the region encompassing all RNA release sites) is large and starts much closer to the promoter than for $_{Ec}$Rho (Figure 6B, compare gel lanes 2 and 3; see also Supplementary Figure S4A) which is consistent with previous observations (25).

Promoter-proximal (early) termination stop points are reminiscent of the behavior of the $_{Mlut}$Rho factor from *M. luteus* which also contains a large hydrophilic subdomain in its NTD (Supplementary Figure S1) (40). Deletion of this subdomain in $_{Mlut}$Rho impairs early termination (48). We thus tested the termination activity of the Δ$_{Mtb}$Rho variant, which lacks the NTD insertion subdomain of $_{Mtb}$Rho, and observed that Δ$_{Mtb}$Rho has a reduced capacity to trigger early termination (Figure 6B, lane 4; Supplementary Figures S4A and S5). By contrast, the $_{[Mtb:Ec]}$Rho chimera triggers strong early termination starting even earlier than WT $_{Mtb}$Rho (Figure 6B, lane 5; Supplementary Figures S4 and S5).

Importantly, the catalytic mutant E386A is unable to trigger efficient transcript release (Figure 6B, lane 6; Supplementary Figure S4A) supporting that ATP hydrolysis is mandatory for transcription termination induced by $_{Mtb}$Rho. By contrast, the T501A mutation only marginally affects transcription termination under our standard conditions by slightly favoring late over early termination (Figure 6B, lane 7; Supplementary Figures S4A and S5). Finally,

the T501K mutant has an increased capacity to trigger early termination but its TE$_{app}$ is not much different from that of WT $_{Mtb}$Rho under our standard experimental conditions (Figure 6B, lane 8 and histogram; see also Supplementary Figures S4A and S5).

To confirm the importance of ATP hydrolysis for the termination activity of $_{Mtb}$Rho, we performed transcription termination experiments in the presence of increasing concentrations of BCM. We observed that BCM inhibits transcription termination induced by $_{Mtb}$Rho in a dose-dependent fashion (Figure 6C; see also Supplementary Figure S4B) but with a global IC$_{50}$ = [289 ± 51] μM that is one order of magnitude higher than for $_{Ec}$Rho (IC$_{50}$ = [27 ± 3] μM). Quantification of termination efficiencies at individual termination positions yielded similar results with individual IC$_{50}$ values ranging between ∼150 and ∼300 μM for $_{Mtb}$Rho and being lower than ∼40 μM for $_{Ec}$Rho (data not shown). Inhibition of the termination activity of the Δ$_{Mtb}$Rho mutant also requires high BCM concentrations (global IC$_{50}$ = [281 ± 29] μM; Figure 6D), ruling out that BCM activity is perturbed significantly by the NTD insertion subdomain in $_{Mtb}$Rho. By contrast, the $_{[Mtb:Ec]}$Rho chimera is inhibited at significantly lower BCM concentrations with a global IC$_{50}$ of [95 ± 13] μM (Figure 6D) and IC$_{50}$ values for individual termination positions as low as ∼40 μM (Supplementary Figure S6). Taken together, these data indicate that $_{Mtb}$Rho has a low apparent affinity for BCM that is due primarily to the composition of its CTD but confirm nonetheless that $_{Mtb}$Rho requires the energy derived from ATP hydrolysis to trigger transcription termination.

Interestingly, the proportion of late (longer than ∼220 nt) termination products formed with the $_{[Mtb:Ec]}$Rho chimera tend to increase at low BCM concentrations which contrasts with the evolution of early termination products (Figure 6D and Supplementary Figure S6). This suggests that sub-inhibitory concentrations of BCM trigger a downstream shift of the termination window, possibly because BCM slows down processive translocation of the $_{[Mtb:Ec]}$Rho chimera and alters its kinetic competition with RNAP (49). This phenomenon is not detected for WT $_{Mtb}$Rho (Figure 6C and data not shown), which seems consistent with its low apparent processivity deduced from helicase experiments (compare Figures 3 and 4A). Hence, BCM-impaired $_{Mtb}$Rho may not remain bound to the nascent transcript for sufficiently long times (and translocated distances) to catch up with RNAP at alternative pausing sites located further away from the initial *Rut* loading site.

DISCUSSION

The mtbRho factor is a *bona fide* molecular motor

Transcription termination factor Rho is widespread in bacteria (13) where it supports important physiological functions linked to Rho-induced disruption of TECs or R-loops (7–9). Many Gram-negative species are sensitive to the antibiotic BCM (9), a naturally occurring, non-competitive inhibitor of Rho's ATPase (20), whereas only one tested Gram-positive species—*M. luteus*—has been found to be sensitive to BCM (16). This spectrum of BCM activity suggested that Rho is dispensable in most Gram-positive bac-
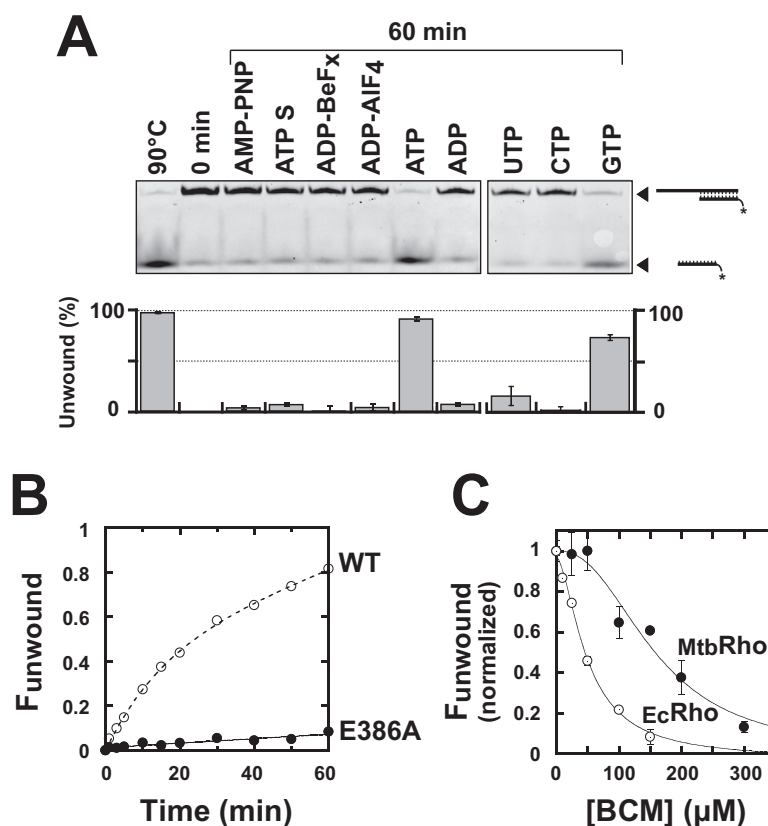
Figure 5. ATP hydrolysis is required for duplex unwinding by $_{Mtb}$Rho. Experiments were performed with substrate C under standard helicase conditions unless specified otherwise. (**A**) Comparison of the activation potential of various nucleotide cofactors (each present at a final concentration of 1 mM). (**B**) The ATPase-deficient mutant E386A does not unwind substrate C efficiently. (**C**) BCM-induced inhibition of the $_{Ec}$Rho (open circles) and $_{Mtb}$Rho (filled circles) helicases. The graph shows the normalized fractions of unwound duplex C formed after 60 min of incubation in the presence of Rho and ATP as a function of the concentration of BCM present in the reaction mixture. Note that BCM has complex effects on the kinetic regimens of the multirun helicase reactions (not shown) which prevent determination of reliable inhibitory parameters based on the evolution of unwinding reaction amplitudes or rates as a function of BCM concentration.

teria, a proposal that has been tested and verified for only a few specimens such as *S. aureus* (17). Recently, an alternative explanation has been proposed for mycobacterial resistance to BCM (25). Based on the observation that $_{Mtb}$Rho disrupted stalled TECs in the presence of AMP-PNP or ATPγS and because the authors failed to detect a significant helicase activity for $_{Mtb}$Rho, they proposed that the enzyme is able to trigger transcription termination by a mechanism uncoupled from molecular motor function (25). Such a mechanism would make $_{Mtb}$Rho intrinsically resistant to BCM, which is what the authors observed for BCM concentrations up to 200 μM (25). Our data, however, do not corroborate this hypothesis and suggest alternative explanations as is discussed below.

Tight RNA binding by a protein is sometimes sufficient to destabilize proximal complexes on RNA. This principle is utilized by DEAD-box proteins which bind ATP and RNA cooperatively to disrupt short RNA duplexes (or RNA:protein complexes) in a non-directional fashion (1,6). However, $_{Mtb}$Rho does not bind RNA much tighter in the presence of nucleotides (Table 1) and differs from DEAD-box proteins by two other important criteria. First, $_{Mtb}$Rho is unable to unwind short duplex substrates in the presence of non-hydrolysable ATP analogs (Figure 5A). Second,

$_{Mtb}$Rho cannot unwind substrates wherein the duplex region is located upstream of the ssRNA loading (e.g. *Rut*) site (Supplementary Figure S3). Rather, the $_{Mtb}$Rho enzyme behaves as a *bona fide* ATP-dependent [5′→3] RNA translocase only able to unwind short RNA duplexes located downstream from a *Rut* site (Figure 3). This activity strictly requires ATP (or GTP) hydrolysis (Figure 5B), a condition confirmed by the inhibition of duplex unwinding induced by the non-conservative mutation of the catalytic Glu$_{386}$ residue (Figure 5B, E386A mutation) or by high concentrations of BCM (Figure 5C). Importantly, *in vitro* transcription termination by $_{Mtb}$Rho is similarly inhibited by the E386A mutation (Figure 6B) or by high BCM concentrations (Figure 6C), supporting that both the helicase and termination functions of $_{Mtb}$Rho proceed by the same motor-dependent mechanism. This conclusion is in apparent contradiction with the previous observation that artificially stalled TECs can be dissociated by $_{Mtb}$Rho in the presence of ATPγS or AMP-PNP (25). However, the reported TEC dissociation rates were low, especially in the presence of AMP-PNP (∼7% of the ATP-dependent rate) (25), and may thus reflect residual motor-independent destabilization as much as experimental limitation(s) due, for instance, to slow hydrolysis of ATPγS by $_{Mtb}$Rho (see 'Results' section)
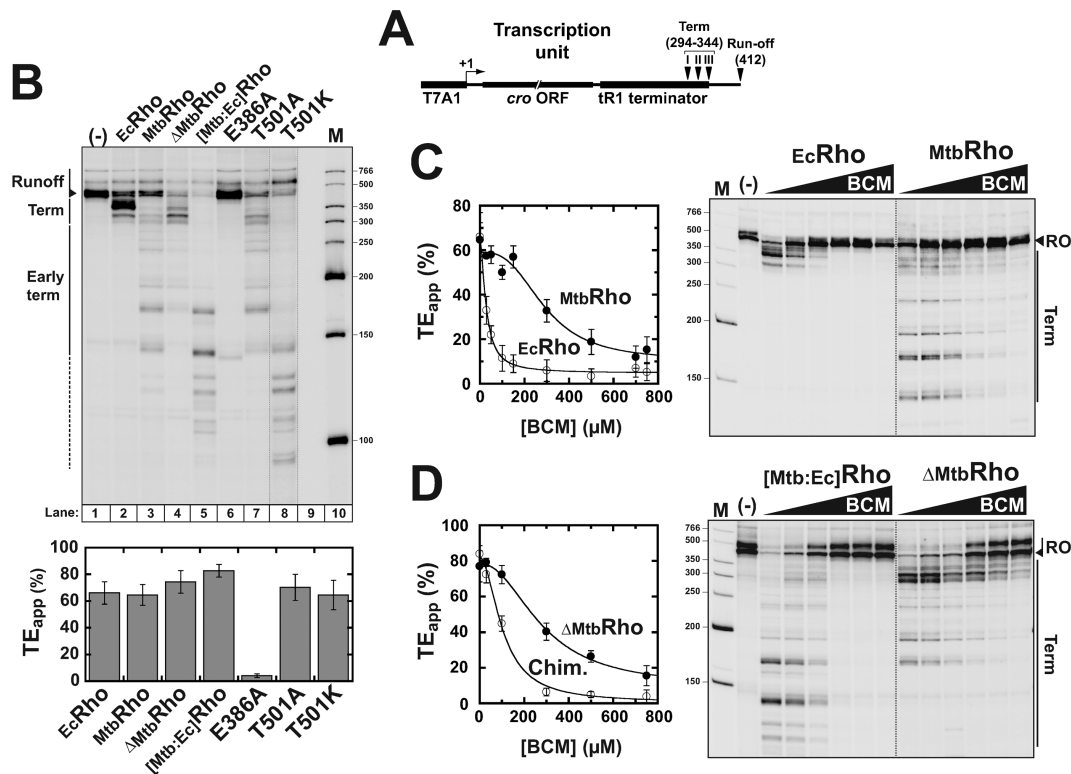
Figure 6. Transcription termination experiments. (**A**) Schematic of the DNA template containing the λtR1 terminator used in *in vitro* termination experiments. (**B**) Both the NTD and CTD of $_{Mtb}$Rho affect its transcription termination activity. A representative denaturing PAGE gel showing the products of transcription termination experiments performed under standard 'chase' conditions with *E. coli* RNAP and the λtR1terminator in the presence of various Rho factors (indicated above gel lanes). Intensity of the T501K lane had to be adjusted separately (as indicated by vertical dotted lines) because reactions with the T501K mutant consistently yielded lower product amounts. Apparent termination efficiencies (TE$_{app}$) are indicated below the gel (N_R = 3). (**C**) A higher concentration of BCM is required to inhibit $_{Mtb}$Rho than $_{Ec}$Rho under standard transcription termination 'chase' conditions (N_R = 3). (**D**) Comparison of the termination activities of the $_{[Mtb:Ec]}$Rho and $_{\Delta Mtb}$Rho variants in the presence of BCM indicates that structural components conferring BCM resistance to $_{Mtb}$Rho are located mostly in its CTD. In the figure, the intensity and gamma settings were adjusted to facilitate the comparison of termination signals in the various gel panels (separated by dotted lines). Gel images without gamma setting adjustments are presented in Supplementary Figures S6 and S7F.

or contamination of commercial AMP-PNP preparations by ATP ([50]).

Limited helicase processivity versus high termination efficiency of mtbRho

Although our data unambiguously demonstrate that $_{Mtb}$Rho is a directional, ATP-fueled RNA helicase, they also show that the enzyme is much less efficient than its $_{Ec}$Rho homolog at unwinding long duplexes (Figure [3]). This low processivity of $_{Mtb}$Rho derives from at least two specific structural features which are discussed below.

First, the presence of a threonine residue (instead of a basic lysine/arginine residue, as in most Rho homologs) ([13]) at the C-terminal position of the R-loop (Thr$_{501}$) most likely weakens the SBS:RNA interaction network in $_{Mtb}$Rho. Replacement of Thr$_{501}$ by a lysine (T501K mutant) enhances the capacity of $_{Mtb}$Rho to unwind longer duplexes whereas its replacement by alanine (T501A mutant) abrogates the unwinding burst observed with a short duplex (Figure [4]B). These observations are consistent with Rho helicase processivity depending on optimal SBS:RNA interactions ([11]). Interestingly, the T501K mutation also strongly favors early termination whereas T501A slightly disfavors it (Figure [6]B;

Supplementary Figure S5). The initial capture of a *Rut* site, which depends on PBS:RNA contacts ([7–9]), should not be affected by modifications of SBS residues. However, subsequent activation of the *Rut*-bound Rho motor may be stimulated by extra (or stronger) SBS:RNA contacts, thereby allowing earlier catch up with RNAP. The superior behavior of the $_{[Mtb:Ec]}$Rho chimera (Figures [4]A and [6]B), which contains the SBS of $_{Ec}$Rho, lends support to this proposal. One should also note that the suboptimal R-loop configuration in $_{Mtb}$Rho probably increases the dependency of the SBS:RNA network on Q-loop contacts. This conjecture is supported by preliminary analysis of Q-loop mutant phenotypes (our unpublished observations). For instance, the single-point S461A mutant of $_{Mtb}$Rho displays a strong (∼10-fold) defect in poly[rC]-dependent ATPase activity (Supplementary Figure S7) whereas the corresponding T286A mutation in the Q-loop of $_{Ec}$Rho only reduces ATPase activity by 35% ([51]). This difference should be considered in light of the fact that Thr$_{286}$ side chains make direct contacts with RNA in the crystal structure of $_{Ec}$Rho ([10]).

Second, the presence of a large, hydrophilic NTD insertion subdomain in $_{Mtb}$Rho (Figure [1]B) appears to perturb

the coupling between RNA binding and motor functions. Deletion of this subdomain (Δ_{Mtb}Rho variant) weakens RNA binding (Table 1) but significantly increases the ATPase turnover and apparent duplex unwinding processivity of $_{Mtb}$Rho at saturating RNA concentrations (see 'Results' section and Figure 4A). Bulky NTD subdomain appendages (Figure 1C) may hamper the structural rearrangements driving enzyme activation and mechanochemical transduction (i.e. transformation of chemical energy into mechanical work) in the Rho ring (10,52). Such constraints are, however, much less detrimental in the $_{[Mtb:Ec]}$Rho chimera which displays processive unwinding (Figure 4A) and strong termination (Figure 6B) activities. The NTD subdomain thus appears to specifically exacerbate the suboptimal behavior of the $_{Mtb}$Rho motor.

We cannot totally exclude that the processivity of the $_{Mtb}$Rho helicase is also mitigated by suboptimal PBS interactions with the duplex substrates. Our synthetic *Rut* sequence has been optimized for $_{Ec}$Rho (30,44) and may thus not adequately recapitulate the distinct features of *M. tuberculosis* transcripts (39). An optimal $_{Mtb}$Rho:*Rut* interaction crowning the Rho hexamer could enhance intersubunit cohesion (and ring stability) during tethered tracking, thereby favoring further RNA translocation over RNA exit from the Rho ring and dissociation (11,12). Comparison of the enzymatic activities of the $_{Mtb}$Rho and $_{[Mtb:Ec]}$Rho factors (Figures 2C, 4A and 6) nonetheless supports that $_{Ec}$Rho contains a stronger, more processive motor than $_{Mtb}$Rho. It thus remains to be seen whether $_{Mtb}$Rho will be able to disrupt stable R-loop structures under appropriate conditions. This capacity could have some value if $_{Mtb}$Rho has to deal with transcriptional R-loops *in vivo*, as is the case for $_{Ec}$Rho (Figure 1A) (53), which is not known yet.

Although $_{Mtb}$Rho efficiently terminates transcription by *E. coli*'s RNAP under conditions that favor fast RNAP translocation (Figure 6A; Supplementary Figure S4), our data suggest that $_{Mtb}$Rho cannot operate far from its loading site on the nascent transcript. This proposal is notably supported by the lack of downstream shift of the $_{Mtb}$Rho termination window in the presence of sub-inhibitory concentrations of BCM (see 'Results' section). We thus propose that, while the processive $_{Ec}$Rho has evolved to catch up with RNAP at sites located up to ~130 nt downstream from the *Rut* region (7–9), $_{Mtb}$Rho needs to promptly inactivate its RNAP target. This task could be facilitated by the significantly lower elongation rate of *M. tuberculosis*' RNAP (54) or by direct interactions between Rho and RNAP (55) that could be stronger in the case of $_{Mtb}$Rho (e.g. due to the NTD insertion subdomain). Further work is necessary to rigorously test these intriguing possibilities.

Origin(s) of BCM resistance

The low apparent affinity of $_{Mtb}$Rho for BCM that was deduced from helicase (Figure 5C) and transcription termination (Figure 6B and C) experiments is intriguing given that $_{Mtb}$Rho does not contain mutations that are known to confer BCM resistance (13). These mutations usually disrupt molecular contacts between amino acids and BCM in the ATPase pocket of Rho, thereby destabilizing the Rho:BCM complex (20). We could not determine BCM affinities by

microcalorimetry because of experimental constraints associated with weak ligand binding (56) and foaming of concentrated $_{Mtb}$Rho solutions in the microcalorimeter mixing chamber (our unpublished observations). Thus, weakening of BCM binding by unknown structural determinants in $_{Mtb}$Rho (e.g. ones that would alter the shape of, or access to, the ATPase pocket) cannot be formally ruled out. Other explanations based on distinctive mechanochemical coupling in $_{Mtb}$Rho are also possible, although their rigorous testing is beyond the scope of the present study.

Conserved transcription termination mechanisms in *M. tuberculosis*

Pathogenic mycobacteria have long adapted their metabolisms and genetic programs to the colonization of harsh and changing environments such as host macrophages and granuloma (57). How this adaptation is enforced at the level of mycobacterial transcription is only fragmentarily understood. The two major pathways leading to transcription termination in bacteria—that is, intrinsic termination and Rho-dependent termination—have been proposed to be markedly distinct in *M. tuberculosis* (25,58). However, a recent study demonstrated that mycobacterial RNAP terminates transcription at canonical intrinsic terminators in a process which can be aided by NusG, as in other bacteria (54). Mycobacterial RNAP only displayed an increased capacity (as compared to *E.coli*'s RNAP) to use terminators with suboptimal U-tracts (54). In the present work, we demonstrate that $_{Mtub}$Rho operates by a canonical 'molecular motor' mechanism that resembles the one used by $_{Ec}$Rho. It thus appears that both intrinsic and factor-dependent termination mechanisms are not fundamentally different in *M. tuberculosis* but adjusted to the characteristics of the bacterium that include a GC-rich genome and slow metabolism. Since $_{Mtub}$Rho is expressed in *M. tuberculosis* (23) and appears to be essential for growth (21,22), seeking $_{Mtub}$Rho inhibitors by using a screening strategy derived from ATP-dependent motor assays (such as the ones presented in this study) could thus prove useful in the fight against tuberculosis, a major and global health concern.

SUPPLEMENTARY DATA

Supplementary Data are available at NAR Online.

REFERENCES

1. Jarmoskaite,I. and Russell,R. (2014) RNA helicase proteins as chaperones and remodelers. *Annu. Rev. Biochem.*, **83**, 697–725.
2. Jankowsky,E. and Fairman-Williams,M.E. (2010) An introduction to RNA helicases: superfamilies, families, and major themes. In: Jankowsky,E (ed). *RNA Helicases*. RSC Publishing, Cambridge, Vol. **19**, pp. 1–31.
3. Steimer,L. and Klostermeier,D. (2012) RNA helicases in infection and disease. *RNA Biol.*, **9**, 751–771.
4. Rabhi,M., Tuma,R. and Boudvillain,M. (2010) RNA remodeling by hexameric RNA helicases. *RNA Biol.*, **7**, 655–666.
5. Singleton,M.R., Dillingham,M.S. and Wigley,D.B. (2007) Structure and mechanism of helicases and nucleic acid translocases. *Annu. Rev. Biochem.*, **76**, 23–50.
6. Linder,P. and Jankowsky,E. (2011) From unwinding to clamping - the DEAD box RNA helicase family. *Nat. Rev. Mol. Cell Biol.*, **12**, 505–516.
7. Boudvillain,M., Figueroa-Bossi,N. and Bossi,L. (2013) Terminator still moving forward: expanding roles for Rho factor. *Curr. Opin. Microbiol.*, **16**, 118–124.
8. Peters,J.M., Vangeloff,A.D. and Landick,R. (2011) Bacterial transcription terminators: the RNA 3′-end chronicles. *J. Mol. Biol.*, **412**, 793–813.
9. Rabhi,M., Rahmouni,A.R. and Boudvillain,M. (2010) Transcription termination factor Rho: a ring-shaped RNA helicase from bacteria. In: Jankowsky,E (ed). *RNA Helicases*. RSC Publishing, Cambridge (UK), Vol. **19**, pp. 243–271.
10. Thomsen,N.D. and Berger,J.M. (2009) Running in reverse: the structural basis for translocation polarity in hexameric helicases. *Cell*, **139**, 523–534.
11. Soares,E., Schwartz,A., Nollmann,M., Margeat,E. and Boudvillain,M. (2014) The RNA-mediated, asymmetric ring regulatory mechanism of the transcription termination Rho helicase decrypted by time-resolved Nucleotide Analog Interference Probing (trNAIP). *Nucleic Acids Res.*, **42**, 9270–9284.
12. Gocheva,V., Le Gall,A., Boudvillain,M., Margeat,E. and Nollmann,M. (2015) Direct observation of the translocation mechanism of transcription termination factor Rho. *Nucleic Acids Res.*, **43**, 2367–2377.
13. D'Heygere,F., Rabhi,M. and Boudvillain,M. (2013) Phyletic distribution and conservation of the bacterial transcription termination factor Rho. *Microbiology*, **159**, 1423–1436.
14. OIE. (2014) List of antimicrobial agents of veterinary importance. *World Organization for Animal Health, Annual Report*. pp. 1–8.
15. Kohn,H. and Widger,W. (2005) The molecular basis for the mode of action of bicyclomycin. *Curr. Drug Targets Infect. Disord.*, **5**, 273–295.
16. Nowatzke,W.L., Keller,E., Koch,G. and Richardson,J.P. (1997) Transcription termination factor Rho is essential for Micrococcus luteus. *J. Bacteriol.*, **179**, 5238–5240.
17. Washburn,R.S., Marra,A., Bryant,A.P., Rosenberg,M. and Gentry,D.R. (2001) rho is not essential for viability or virulence in Staphylococcus aureus. *Antimicrob. Agents Chemother.*, **45**, 1099–1103.
18. Van Bambeke,F., Glupczynski,Y., Plesiat,P., Pechere,J.C. and Tulkens,P.M. (2003) Antibiotic efflux pumps in prokaryotic cells: occurrence, impact on resistance and strategies for the future of antimicrobial therapy. *J. Antimicrob. Chemother.*, **51**, 1055–1065.
19. Magyar,A., Zhang,X., Kohn,H. and Widge,W.R. (1996) The antibiotic bicyclomycin affects the secondary RNA binding site of Escherichia coli transcription termination factor Rho. *J. Biol. Chem.*, **271**, 25369–25374.
20. Skordalakes,E., Brogan,A.P., Park,B.S., Kohn,H. and Berger,J.M. (2005) Structural mechanism of inhibition of the Rho transcription termination factor by the antibiotic bicyclomycin. *Structure*, **13**, 99–109.
21. Griffin,J.E., Gawronski,J.D., Dejesus,M.A., Ioerger,T.R., Akerley,B.J. and Sassetti,C.M. (2011) High-resolution phenotypic profiling defines genes essential for mycobacterial growth and cholesterol catabolism. *PLoS Pathogens*, **7**, e1002251.
22. Sassetti,C.M., Boyd,D.H. and Rubin,E.J. (2003) Genes required for mycobacterial growth defined by high density mutagenesis. *Mol. Microbiol.*, **48**, 77–84.
23. Wolfe,L.M., Veeraraghavan,U., Idicula-Thomas,S., Schurer,S., Wennerberg,K., Reynolds,R., Besra,G.S. and Dobos,K.M. (2013) A chemical proteomics approach to profiling the ATP-binding proteome of Mycobacterium tuberculosis. *Mol. Cell. Proteomics*, **12**, 1644–1660.
24. Nishida,M., Mine,Y., Matsubara,T., Goto,S. and Kuwahara,S. (1972) Bicyclomycin, a new antibiotic. 3. In vitro and in vivo antimicrobial activity. *J. Antibiot. (Tokyo)*, **25**, 582–593.
25. Kalarickal,N.C., Ranjan,A., Kalyani,B.S., Wal,M. and Sen,R. (2010) A bacterial transcription terminator with inefficient molecular motor action but with a robust transcription termination function. *J. Mol. Biol.*, **395**, 966–982.
26. Boudvillain,M., Walmacq,C., Schwartz,A. and Jacquinot,F. (2010) Simple enzymatic assays for the in vitro motor activity of transcription termination factor Rho from Escherichia coli. *Methods Mol. Biol.*, **587**, 137–154.
27. Rabhi,M., Gocheva,V., Jacquinot,F., Lee,A., Margeat,E. and Boudvillain,M. (2011) Mutagenesis-based evidence for an asymmetric configuration of the ring-shaped transcription termination factor Rho. *J. Mol. Biol.*, **405**, 497–518.
28. D'Heygere,F., Schwartz,A., Coste,F., Castaing,B. and Boudvillain,M. (2015) Monitoring RNA Unwinding by the Transcription Termination Factor Rho from Mycobacterium tuberculosis. *Methods Mol. Biol.*, **1259**, 293–311.
29. Gan,E. and Richardson,J.P. (1999) ATP and other nucleotides stabilize the Rho-mRNA complex. *Biochemistry*, **38**, 16882–16888.
30. Walmacq,C., Rahmouni,A.R. and Boudvillain,M. (2004) Influence of substrate composition on the helicase activity of transcription termination factor Rho: reduced processivity of Rho hexamers during unwinding of RNA-DNA hybrid regions. *J. Mol. Biol.*, **342**, 403–420.
31. Schwartz,A., Walmacq,C., Rahmouni,A.R. and Boudvillain,M. (2007) Noncanonical interactions in the management of RNA structural blocks by the transcription termination rho helicase. *Biochemistry*, **46**, 9366–9379.
32. Walmacq,C., Rahmouni,A.R. and Boudvillain,M. (2006) Testing the steric exclusion model for hexameric helicases: substrate features that alter RNA-DNA unwinding by the transcription termination factor Rho. *Biochemistry*, **45**, 5885–5895.
33. Figueroa-Bossi,N., Schwartz,A., Guillemardet,B., D'Heygere,F., Bossi,L. and Boudvillain,M. (2014) RNA remodeling by bacterial global regulator CsrA promotes Rho-dependent transcription termination. *Genes Dev.*, **28**, 1239–1251.
34. Rabhi,M., Espeli,O., Schwartz,A., Cayrol,B., Rahmouni,A.R., Arluison,V. and Boudvillain,M. (2011) The Sm-like RNA chaperone Hfq mediates transcription antitermination at Rho-dependent terminators. *Embo J.*, **30**, 2805–2816.
35. Burton,M.E. (2006) *Applied pharmacokinetics & pharmacodynamics: principles of therapeutic drug monitoring*. 4th edn. Lippincott Williams & Wilkins, Baltimore, MD.
36. Canals,A., Uson,I. and Coll,M. (2010) The structure of RNA-free Rho termination factor indicates a dynamic mechanism of transcript capture. *J. Mol. Biol.*, **400**, 16–23.
37. Skordalakes,E. and Berger,J.M. (2003) Structure of the Rho transcription terminator: mechanism of mRNA recognition and helicase loading. *Cell*, **114**, 135–146.
38. Balasubramanian,K. and Stitt,B.L. (2010) Evidence for amino acid roles in the chemistry of ATP hydrolysis in Escherichia coli Rho. *J. Mol. Biol.*, **404**, 587–599.
39. Mitra,A., Misquitta,R. and Nagaraja,V. (2014) Mycobacterium tuberculosis Rho Is an NTPase with distinct kinetic properties and a novel RNA-binding subdomain. *PLoS One*, **9**, e107474.
40. Nowatzke,W.L. and Richardson,J.P. (1996) Characterization of an unusual Rho factor from the high G + C Gram-positive bacterium Micrococcus luteus. *J. Biol. Chem.*, **271**, 742–747.
41. Ingham,C.J., Hunter,I.S. and Smith,M.C. (1996) Isolation and sequencing of the rho gene from Streptomyces lividans ZX7 and characterization of the RNA-dependent NTPase activity of the overexpressed protein. *J. Biol. Chem.*, **271**, 21803–21807.

42. Bustamante,C., Cheng,W. and Mejia,Y.X. (2011) Revisiting the central dogma one molecule at a time. *Cell*, **144**, 480–497.

43. Cummins,L.L., Owens,S.R., Risen,L.M., Lesnik,E.A., Freier,S.M., McGee,D., Guinosso,C.J. and Cook,P.D. (1995) Characterization of fully 2′-modified oligoribonucleotide hetero- and homoduplex hybridization and nuclease sensitivity. *Nucleic Acids Res.*, **23**, 2019–2024.

44. Guerin,M., Robichon,N., Geiselmann,J. and Rahmouni,A.R. (1998) A simple polypyrimidine repeat acts as an artificial Rho-dependent terminator in vivo and in vitro. *Nucleic Acids Res.*, **26**, 4895–4900.

45. Yang,Q. and Jankowsky,E. (2006) The DEAD-box protein Ded1 unwinds RNA duplexes by a mode distinct from translocating helicases. *Nat. Struct. Mol. Biol.*, **13**, 981–986.

46. Liu,F., Putnam,A. and Jankowsky,E. (2008) ATP hydrolysis is required for DEAD-box protein recycling but not for duplex unwinding. *Proc. Natl. Acad. Sci. U.S.A.*, **105**, 20209–20214.

47. Liu,F., Putnam,A.A. and Jankowsky,E. (2014) DEAD-box helicases form nucleotide-dependent, long-lived complexes with RNA. *Biochemistry*, **53**, 423–433.

48. Nowatzke,W.L., Burns,C.M. and Richardson,J.P. (1997) Function of the novel subdomain in the RNA binding domain of transcription termination factor Rho from Micrococcus luteus. *J. Biol. Chem.*, **272**, 2207–2211.

49. Jin,D.J., Burgess,R.R., Richardson,J.P. and Gross,C.A. (1992) Termination efficiency at rho-dependent terminators depends on kinetic coupling between RNA polymerase and rho. *Proc. Natl. Acad. Sci. U.S.A.*, **89**, 1453–1457.

50. Meyer,A.S., Gillespie,J.R., Walther,D., Millet,I.S., Doniach,S. and Frydman,J. (2003) Closing the folding chamber of the eukaryotic chaperonin requires the transition state of ATP hydrolysis. *Cell*, **113**, 369–381.

51. Wei,R.R. and Richardson,J.P. (2001) Mutational changes of conserved residues in the Q-loop region of transcription factor Rho greatly reduce secondary site RNA-binding. *J. Mol. Biol.*, **314**, 1007–1015.

52. Stitt,B.L. and Xiao,H. (2010) Conformation changes in E. coli Rho monitored by hydrogen/deuterium exchange and mass spectrometry: response to ligand binding. *J. Mol. Biol.*, **402**, 813–824.

53. Krishna Leela,J., Syeda,A.H., Anupama,K. and Gowrishankar,J. (2013) Rho-dependent transcription termination is essential to prevent excessive genome-wide R-loops in Escherichia coli. *Proc. Natl. Acad. Sci. U.S.A.*, **110**, 258–263.

54. Czyz,A., Mooney,R.A., Iaconi,A. and Landick,R. (2014) Mycobacterial RNA polymerase requires a U-tract at intrinsic terminators and is aided by NusG at suboptimal terminators. *mBio*, **5**, e00931.

55. Epshtein,V., Dutta,D., Wade,J. and Nudler,E. (2010) An allosteric mechanism of Rho-dependent transcription termination. *Nature*, **463**, 245–249.

56. Brogan,A.P., Widger,W.R., Bensadek,D., Riba-Garcia,I., Gaskell,S.J. and Kohn,H. (2005) Development of a technique to determine bicyclomycin-rho binding and stoichiometry by isothermal titration calorimetry and mass spectrometry. *J. Am. Chem. Soc.*, **127**, 2741–2751.

57. Cambier,C.J., Falkow,S. and Ramakrishnan,L. (2014) Host evasion and exploitation schemes of mycobacterium tuberculosis. *Cell*, **159**, 1497–1509.

58. Unniraman,S., Prakash,R. and Nagaraja,V. (2001) Alternate paradigm for intrinsic transcription termination in eubacteria. *J. Biol. Chem.*, **276**, 41850–41855.